International Journal of Automotive Technology, Vol. 16, No. 1, pp. 1–15 (2015)
DOI 10.1007/s12239–015–0001–x

pISSN 1229–9138/ eISSN 1976–3832

3D EHD LUBRICATION AND WEAR FOR PISTON RING-CYLINDER LINER ON DIESEL ENGINES

Y. K. JIANG[1)*], J. P. ZHANG[1, 2)], G. HONG[3)], L. P. WAN[1)] and X. LIU[1)]

[1)]School of Energy and Power Engineering, Huazhong University of Science and Technology, Wuhan 430074, China
[2)]School of Mechanical Engineering, Xiangtan University, Xiangtan 411105, China
[3)]School of Electronics, Mechanics and Mechatronic Systems, University of Technology, Sydney NSW 2007, Australia

(Received 15 May 2013; Revised 13 October 2013; Accepted 11 November 2013)

ABSTRACT–The three-dimensional EHD lubrication and wear loss of piston ring-cylinder liner components for five rings in the firing diesel engine was studied by using VC++ programs. The gas blowby, variable density and viscosity of lubricant, the surface roughness, friction heat flux and the normal elastic deformation are all considered in the EHD lubrication analysis algorithm. Meanwhile, the wear loss of the cylinder liner was also calculated when the diesel was started under cold starting condition in which the wearing was more serious than that in warm starting condition. The simulated results were compared with the wear measurement of the cylinder liner, and they matched well. It was found that the hydrodynamic friction force was larger than the asperity friction force, and the wear distribution of the barrel piston ring was very different from that of the rectangular piston ring. The distribution trend of the nominal oil film thickness was similar to the normal elastic deformation, but opposite to the wear loss of the piston rings. The wear loss caused by the first piston ring was the biggest and played a dominant role in the wear loss of cylinder liner. The greatest wear loss of the cylinder liner occurs at the time near top dead centre.

KEY WORDS : Elastohydrodynamic lubrication, Modified average reynolds equation, Adhesive wear, Piston ring-cylinder liner, Firing diesel engine

NOMENCLATURE

a_c : piston acceleration, m/s^2
A : apparent area of contact, m^2
A_1~A_5 : blowby area of five ring gaps, m^2
A_c : real area of contact, m^2
b : effective axial height of the piston ring, m
C_A, C_B, D_t: empirical parameter of density-pressure
E' : comprehensive elastic modulus, Pa
E_1 : elastic modulus of piston ring, Pa
E_2 : elastic modulus of cylinder liner, Pa
F_1 : gas force acting on the leading edge of the piston ring, N
F_2 : gas force acting on the trailing edge of the piston ring, N
F_e : elastic force of the piston ring, N
F_r : radial friction force acting on the piston ring, N
F_t : axial viscosity friction force acting on the piston ring, N
F_x : axial hydrodynamic force acting on the piston ring, N
F_A : friction force caused by shearing of asperities, N
F_G : total gas force acting on the back of the piston ring, N
F_Z : normal hydrodynamic force acting on the piston ring radially, N
g : gravity constant = 9.81, m/s^2
h : nominal oil film thickness, m
h_0 : minimum oil film thickness, m
h_x : axial variation of oil film thickness, m
h_y : circumferential variation of oil film thickness, m
h_T : actual oil film thickness, m
H : film thickness ratio, $H = h/\sigma$
k : gas specific heat
K_c : gas flow coefficient
L : circumferential length of the piston ring, m
Mg : gravity of piston ring, N
p : oil film pressure, Pa
$\bar{p}$: average oil film pressure, Pa
p_0 : gas pressure in the crankcase, Pa
p_1~p_4 : inter-ring gas pressure, Pa
p_i : cylinder pressure, Pa
p_R : Reolands' reference pressure, Pa
$p_1(t)$: gas pressure acting on the leading edge of the piston ring, Pa
$p_2(t)$: gas pressure acting on the trailing edge of the piston ring, Pa
R_g : gas constant = 8.314, J/mol K
R_x : groove's axial reaction force acting on the piston

*Corresponding author. e-mail: jykhust@mail.hust.edu.cn

ring, N
S_0 : Roelands' viscosity-temperature coefficient
t : time, s
T : oil film temperature, °C
T_0 : ambient temperature, °C
T_1~T_4 : gas temperature of the four air chambers, °C
T_R : Reolands' reference temperature, °C
U : the relative velocity between the piston ring and cylinder liner, m/s
$v(x, y)$: normal elastic deformation, m
V_1~V_4 : volume of the four air chambers, m^3
V_{r1} : a scale factor, $V_{r1} = (\sigma_1/\sigma)^2$
W_f~W_4 : blowby among five piston ring gap, kg/s
W_A : asperity contact load, N
x : axial coordinate, m
x_c : rupture location of oil film, m
x_i : inlet location of lubricant, m
x_o : outlet location of lubricant, m
y : circumferential coordinate, m
z : Roelands' viscosity-pressure coefficient
α_0 : boundary friction coefficient
β : radius of curvature at peak of asperity, m
δ_1 : random roughness amplitudes of piston ring, m
δ_2 : random roughness amplitudes of cylinder liner, m
κ : wear constant of the lubricant
μ : lubricant viscosity, Pa.s
μ_0 : lubricant viscosity at atmosphere pressure and ambient temperature, Pa.s
μ_R : Roelands' reference viscosity, Pa.s
ν_1 : Poisson's ratio of piston ring
ν_2 : Poisson's ratio of cylinder liner
ρ : lubricant density, kg/m^3
ρ_0 : lubricant density at atmosphere pressure and ambient temperature, kg/m^3
σ : comprehensive roughness, m
σ_1 : roughness of piston ring, m
σ_2 : roughness of cylinder liner, m
σ_s : yield limits of material, Pa
τ_0 : shear strength constant
η : density of asperity
ϕ_c : a dimensionless factor
ϕ_f, ϕ_{fs} : shear stress factor
ϕ_x : pressure flow factor in x direction
ϕ_y : pressure flow factor in y direction
ϕ_s : shear flow factor
φ : crank angle, °

1. INTRODUCTION

Piston ring-cylinder liner components play an important role in the performance evaluation and life prediction, since their lubrication performance and wear loss affect the power and economic performance of a diesel engine. Approximately 50–60 percent of the total mechanical loss of an engine is caused by the friction and wear between the piston ring and cylinder liner. The friction of the piston ring-cylinder liner has been studied extensively in order to improve the lubrication performance and reduce the wear loss. There are lots of factors influenced the calculation of the oil film thickness, such as the shape of the piston ring/ cylinder liner, elastic deformation, friction heat, lubricant viscosity and gas blowby and so on (Liu *et al*., 1998; Yang and Keith, 1996a; Qasim *et al*., 2011). In the early, the hydrodynamic lubrication of piston rings was discussed and summarized when the piston rings were operating in both circular and distorted bores (Ma *et al*., 1997), but the contact surface was assumed to be rigid. The effect of the elliptical cylinder liner and friction heat on the piston ring pack was taken into account in the lubrication analysis of the gasoline engine. The result shows that the elastic deformation significantly affects the tribological performance of piston ring (Ye *et al*., 2003; Ye *et al*., 2004). The early two-dimensional piston ring lubrication study is gradually transformed to the three-dimensional problem. A coupled 3D transient heat transfer model for the moving piston pack- cylinder line was developed, and the effect of the 3D friction heat generated at the piston ring/cylinder liner contact interfaces and the multi-dimensional lubricant film thickness has been considered in the gasoline engine (Jiang *et al*., 2007), but the wear loss was ignored. The model that can predict the frictional losses of each piston pack component was implemented using MATLAB/SIMULINK and the effect of engine speed and engine load on predicted piston pack friction losses was examined (Livanos and Kyrtatos, 2007), however, the friction heat and gas blowby were not considered. A dimensionless Reynolds equation based on a "double-Newtonian" rheology had been derived in the piston ring cylinder wall contact model (Charles *et al*., 2010), while the piston ring pack of the realistic engine was not calculated. The correlation between cavitation and starvation in the vicinity of the top dead centre (TDC) and bottom dead centre (BDC) was investigated (Chong *et al*., 2011), and the top compression ring was used merely. The pressure distribution and oil film thickness of the dynamic bearing were analyzed by integrating an elastohydrodynamic lubrication model with multi-flexible-body dynamics (Choi *et al*., 2012). The adhesive wear of piston ring and cylinder liner in the engine was studied on the basis of lubrication analysis (Zhang *et al*., 2010), but the two compression rings and two oil rings were assumed to have the same lubrication performance and wear loss during the computation process. Additionally, the blowby, the friction force, friction heat flux and the elastic deformation were not discussed in detail.

It is very difficult to study the lubrication and wear performance through experiment and measurement system, especially for the fired engine. Most of previous researchers used the simulative reciprocating motion device (Truhan *et al*., 2005; Kapsiz *et al*., 2011; Johansson *et al*., 2011) to test the lubrication and wear parameters, and then the complex working process of the real engine can not be considered

seriously. The friction force measurement system (Cho *et al*., 2000) was based on the floating liner method, and the cylinder wall roughness, oil starvation and cylinder pressure were all neglected. The flow rate of lubricant had been measured by adding a hydrocarbon marker (Stark *et al*., 2005) to the oil in the sump, while the distribution rule along the piston ring was not observed. The formation and development of the oil film (Tamminen *et al*., 2006) under different load conditions was studied through test instruments. Meanwhile, the simulation results were compared with experimental results, but the varying trends of the oil film thickness along both the axial and circumferential direction of the whole piston ring, the friction force and wear loss were not given. The capacitance method (Dhara *et al*., 2009) is developed for measurement of minimum oil film thickness in a motored engine. In recent years, the micro surface topography (Michalski and Wos, 2011) was focused on the abrasive wear of piston-cylinder liner, and it will be used in the manufacturing process to make the engines more durable and reliable.

However, in the published research work on the lubrication of piston ring-cylinder liner, most of studies are focused on parts of influence factors, and the other factors were neglected. For example, the elastic deformation, gas blowby and asymmetry in the circumferential direction were ignored. In addition, some of studies are based on the reciprocating motion device, in comparison to the firing engine, the friction heat and combustion process are simplified. The blowby pattern is also simple since the ring pack generally consists of three rings. The main goal of this paper is to gain the three-dimensional distribution rules of lubrication parameters and wear loss in the real diesel engine with five piston rings, and compare the wear loss of cylinder liner under warm start condition and cold start condition by simulation and experiment.

In this paper, the 3D calculation model for lubrication performance and investigation to the wear loss of piston ring-cylinder liner for diesel engine are reported. In this model, the piston ring pack is composed of five piston rings, as shown in Figure 1. The first ring is the barrel piston ring and all the other rings are the rectangular piston rings. The input parameters in this model are listed in Table 1. The gas blowby of piston ring gap, friction heat, the normal elastic deformation and surface roughness were all taken into consideration in the algorithm. Additionally, the wear loss of cylinder liner when the firing diesel engine was run under cold start condition was also simulated, and the result was compared with the wear loss when the firing diesel engine was run under warm start condition. The simulated results were verified by comparing the wear measured and that in 2D simulation using AVL code. Finally, the wear losses of different piston rings were compared and some conclusions were drawn.

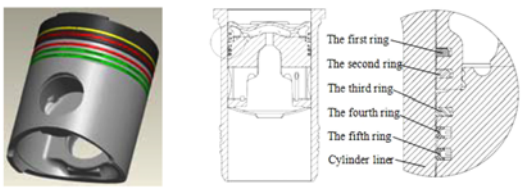

Figure 1. Piston pack of the five rings diesel engine.

Table 1. Physical parameters of piston ring-cylinder liner for the diesel engine.

Physical parameter	Value
Diameter of liner	280[mm]
Gap width of rings	2.4, 1.1, 1.1[mm]
Axial height of ring	4.4, 5, 1.4[mm]
Radial width of rings	9.4, 10.4, 6[mm]
Back height of ring	6, 6, 1.4[mm]
Height of barrel shape	0.016, 0, 0[mm]
Elastic modulus of the ring	206, 160, 206[GPa]
Elastic modulus of cylinder liner	175[GPa]
Density of the ring	7300,7200,7260[kg/m^3]
Poisson's ratio of cylinder liner	0.27
Connecting rod length	570[mm]
Stroke	290[mm]
Rotational speed	1050[r/min]
Total cycles	3.15×10^7
Lubricant density	925[kg/m^3]
Lubricant viscosity	0.13829[Pa.s]
Liner roughness	1.8[um]
Ring roughness	0.4[um]
Density of cylinder liner	7800[kg/m^3]
Poisson's ratio of the ring	0.3, 0.28, 0.25
The blowby area of five rings	0.864,0.385,0.715,0.605, 1.265[mm^2]

2. THREE-DIMENSIONAL COMPUTATIONAL MODEL OF ELASTOHYDRODYNAMIC LUBRICATION

2.1. Modified Average Reynolds Equation

For simplicity, the lubrication between a piston ring and the cylinder liner was modeled by that of a dynamically loaded slider reciprocating over a plane surface, as shown in Figure 2.

The lubricating oil is assumed to be Newtonian fluid and isothermal lubricant, oil film pressure and temperature is a constant along the direction of the oil film thickness since the lubricant thickness is very thin. The oil film thickness is much smaller than the radius of curvature of the adjacent

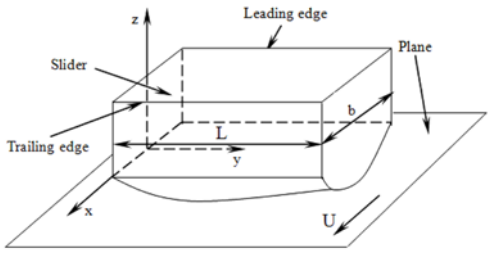

Figure 2. Simple slider-plane model for piston-cylinder liner lubrication simulation.

piston ring and cylinder liner. The flow of lubricant is considered as laminar flow, and no sliding occurs on the solid boundary surface. Equation (1) is the modified average Reynolds equation adopted to simulate the elastohydrodynamic (EHD) lubrication (Ye *et al*., 2003; Ye *et al*., 2004).

$$\frac{\partial}{\partial x}\left(\phi_x\frac{\rho h^3}{\mu}\frac{\partial \bar{p}}{\partial x}\right)+\frac{\partial}{\partial y}\left(\phi_y\frac{\rho h^3}{\mu}\frac{\partial \bar{p}}{\partial y}\right)= 6U\rho\phi_c\frac{\partial h}{\partial x}+6U\sigma\frac{\partial(\rho\phi_s)}{\partial x}+12\rho\phi_c\frac{\partial h}{\partial x} \quad (1)$$

where ϕ_x and ϕ_y are the pressure flow factors in x direction and y direction respectively. ϕ_s is the shear flow factor, $\bar{p}$ is the average oil film pressure, h is the nominal oil film thickness, U is the relative velocity between the piston ring and cylinder liner. σ is the comprehensive roughness, $\sigma=\sqrt{\sigma_1^2+\sigma_2^2}$, where, σ_1 and σ_2 is the roughness of piston ring and cylinder liner respectively. ϕ_c is a dimensionless factor, and is formulated as follow,

$$\phi_c=\begin{cases}\exp(-0.6912+0.782H-0.304H^2+0.0401H^3), 0\le H<3\\ 1, H\ge 3\end{cases} \quad (2)$$

where H is the film thickness ratio, $H=\frac{h}{\sigma}$.

In the process of elastic hydrodynamic lubrication analysis, the variable lubricant viscosity and density must be taken into account. Both the lubricant viscosity and the lubricant density are the explicit function of the pressure and temperature. The lubricant viscosity and density increase with the increasing pressure, but decrease as the temperature increases. Equation (3) is for calculating the variable viscosity of the lubricant and Equation (4) for variable density of the lubricant (Ye *et al*., 2003).

$$\mu=\mu_0\ exp\left\{\ln\left(\frac{\mu_0}{\mu_R}\right)\left[\left(1+\frac{p}{p_R}\right)^z\left(\frac{T-T_R}{T_0-T_R}\right)^{-S_0}-1\right]\right\} \quad (3)$$

$$\frac{\rho}{\rho_0}=1+\frac{C_A p}{1+C_B p}+D_t\,(T-T_0) \quad (4)$$

where μ_0 and ρ_0 is the lubricant viscosity and density at atmosphere pressure and ambient temperature, respectively. p is the oil film pressure, T is the oil film temperature, T_0 is the ambient temperature, T_R is the Reolands' reference temperature, μ_R is the Roelands' reference viscosity, S_0 is the Roelands' viscosity-temperature coefficient, Z is the Roelands' viscosity-pressure coefficient, p_R is the Reolands' reference pressure, C_A, C_B, D_t are empirical parameters of density-pressure, $C_A=0.6\times10^{-9}$, $C_B=1.7\times10^{-9}$, $D_t=-0.0007$.

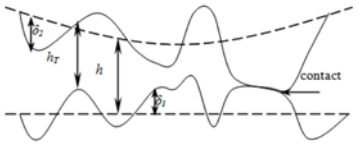

Figure 3. Film thickness function and surface roughness.

2.2. Elastic Deformation and Oil Film Thickness

In practice, the surfaces of the rings and cylinder liner will be deformed when the hydrodynamic pressure is applied. To simulate this deformation, a semi-infinite large elastic body on which a differential concentrated load $p(x, y)$ acts is assumed. Based on elasticity theory, the total surface deformation of the ring and cylinder liner can be modelled by solving Equations (5) and (6). The detailed derivation can be found in reference (Yang and Keith, 1996b).

$$v\,(x_0,\,y_0)=\frac{1}{\pi E'}\iint_A\frac{p(x,y)}{\sqrt{(x-x_0)^2+(y-y_0)^2}}\,dxdy \quad (5)$$

$$E'=\left(\frac{1-\nu_1^2}{E_1}+\frac{1-\nu_2^2}{E_1}\right)^{-1} \quad (6)$$

The nominal oil film thickness h is defined as the distance between the mean levels of the two surfaces and described by Equation (7).

$$h=h_0+h_x+h_y+v(x,\,y) \quad (7)$$

where, h_0 is the minimum oil film thickness, an important adjustable parameter for the convergence of load in the process of computation. h_x and h_y are variations of oil film thickness in axial and circumferential directions respectively. $v(x, y)$ is the normal elastic deformation of the piston ring and cylinder liner due to the hydrodynamic pressure.

The actual oil film thickness h_T and the nominal oil film thickness h are illuminated in Figure 3 in which $h_T=h+\delta_1+\delta_2$ and δ_2 denote random roughness amplitudes of the two surfaces measured from their mean levels.

2.3. Asperity Contact Model and Patterns of Blowby

The forces acting on the piston ring in diesel engines are very complex, including friction force, asperity force, hydrodynamic forces, etc. Figure 4 shows all the forces exerting on a piston ring, including gas forces F_1, F_2 and F_G, hydrodynamic forces F_x, F_t and F_z, surface asperity forces F_A, W_A and F_r, body forces Mg and F_e and reaction force R_x. Ma_c represents the so-called inertial force caused by the acceleration of the piston (ring), and a_c is the acceleration of piston.

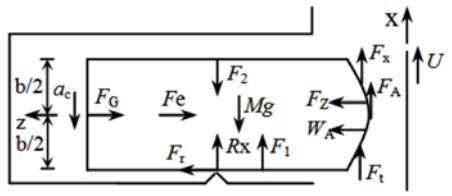

Figure 4. Force analysis of the piston ring.

Equation (8) is the force equilibrium equation in the axial direction.

$$R_x+F_1+F_x+F_t+F_A+Ma_c=F_2+Mg \tag{8}$$

The total friction force in the mixed lubrication region is computed with Equation (9).

$$F=F_A+(F_x+F_t)=\tau_0A_c+\alpha_0W_A +\iint_A\frac{\mu U}{h}[(\phi_f-\phi_{fs})+2V_{r1}\phi_{fs}]dxdy \tag{9}$$

where, τ_0 is a shear strength constant, α_0 is the boundary friction coefficient, ϕ_f, ϕ_{fs} are shear stress factors, and V_{r1} is a scale factor, $V_{r1}=(\sigma_1/\sigma)^2$. F_A, F_x and F_t denote shear force of asperities, viscous friction force due to the hydrodynamic shear stress and the horizontal components of contact pressure, respectively. According to Greenwood and Tripp's asperity contact model, the total force generated by the asperity contact, W_A, and the real area of contact, A_c, are calculated with Equation (10).

$$W_A=(16\sqrt{2}/15)\pi(\eta\beta\sigma)^2E'\sqrt{\sigma/\beta}\,AF_{2.5}(H)$$
$$A_c=\pi^2(\eta\beta\sigma)^2AF_2(H) \tag{10}$$

In which, η is the density of asperity, and β is the radius of curvature at peak of asperity. A_c is real area of contact and A is apparent area of contact. $F_2(H)$ and $F_{2.5}(H)$ are the functions of the film thickness ratio H, and they are formulated as follows,

$$F_2(H)=\begin{cases}1.705\times10^{-4}\exp(4.05419\ln(4.0-H)\\ +1.37025(\ln(4.0-H))^2), & H\le3.5\\ 8.8123\times10^{-5}(4.0-H)^{2.1523}, & 3.5<H\le4\\ 0, & H>4\end{cases} \tag{11}$$

$$F_{2.5}(H)=\begin{cases}2.1339\times10^{-4}\exp(3.804467\ln(4.0-H)\\ +1.341516(\ln(4.0-H))^2), & H\le3.5\\ 1.1201\times10^{-4}(4.0-H)^{1.9447}, & 3.5<H\le4\\ 0, & H>4\end{cases} \tag{12}$$

Equation (13) is the force equilibrium equation in the radial direction.

$$F_G+F_e=F_Z+W_A+F_r \tag{13}$$

Where, F_G is the total gas force acting on the back of the piston ring, F_e is the elastic force of the piston ring, F_z is the normal hydrodynamic force acting on the piston ring radially, and $F_z=\iint_A\bar{p}dxdy$. F_r is the radial friction force generated by the radial movement of the piston ring in the groove, comparison with other radial force, F_r is very small, and it can be negligible, so the radial force balance equation can be formulated:

$$F_G+F_e=F_Z+W_A \tag{14}$$

This study is based on the assumption that the gas blowby of the combustion chamber is the unsteady adiabatic flow, and it meets the state equation of ideal gas and the mass continuity equation. There may be 32 (2^5) types of blowby patterns among the piston pack in the diesel engine, as shown in Figure 5.

Figure 5. 32 types of blowby patterns among the piston rings.

When the first type of blowby patterns occurs, namely, $p_i>p_1$, $p_1>p_2$, $p_2>p_3$, $p_3>p_4$, $p_4>p_0$, the gas flow differential equations through every piston ring gap can be built as follows

$$\frac{dW_1}{dt}=\begin{cases}K_cA_1\sqrt{\frac{2gk}{R_g(k-1)T_i}}p_i\left(\frac{p_1}{p_i}\right)^{\frac{1}{k}}\sqrt{1-\left(\frac{p_1}{p_i}\right)^{\frac{k-1}{k}}} & \frac{p_1}{p_i}>0.546\\ K_cA_1\sqrt{\frac{2gk}{R_g(k-1)T_i}}p_i(0.227) & \frac{p_1}{p_i}\le0.546\end{cases};$$

$$\frac{dW_2}{dt}=\begin{cases}K_cA_2\sqrt{\frac{2gk}{R_g(k-1)T_1}}p_1\left(\frac{p_2}{p_1}\right)^{\frac{1}{k}}\sqrt{1-\left(\frac{p_2}{p_1}\right)^{\frac{k-1}{k}}} & \frac{p_2}{p_1}>0.546\\ K_cA_2\sqrt{\frac{2gk}{R_g(k-1)T_1}}p_1(0.227) & \frac{p_2}{p_1}\le0.546\end{cases};$$

$$\frac{dW_3}{dt}=\begin{cases}K_cA_3\sqrt{\frac{2gk}{R_g(k-1)T_2}}p_2\left(\frac{p_3}{p_2}\right)^{\frac{1}{k}}\sqrt{1-\left(\frac{p_3}{p_2}\right)^{\frac{k-1}{k}}} & \frac{p_3}{p_2}>0.546\\ K_cA_3\sqrt{\frac{2gk}{R_g(k-1)T_2}}p_2(0.227) & \frac{p_3}{p_2}\le0.546\end{cases};$$

$$\frac{dW_4}{dt}=\begin{cases}K_cA_4\sqrt{\frac{2gk}{R_g(k-1)T_3}}p_3\left(\frac{p_4}{p_3}\right)^{\frac{1}{k}}\sqrt{1-\left(\frac{p_4}{p_3}\right)^{\frac{k-1}{k}}} & \frac{p_4}{p_3}>0.546\\ K_cA_4\sqrt{\frac{2gk}{R_g(k-1)T_3}}p_3(0.227) & \frac{p_4}{p_3}\le0.546\end{cases};$$

$$\frac{dW_4}{dt}=\begin{cases}K_c A_5\sqrt{\dfrac{2gk}{R_g(k-1)T_4}}p_4\left(\dfrac{p_0}{p_4}\right)^{\frac{1}{k}}\sqrt{1-\left(\dfrac{p_0}{p_4}\right)^{\frac{k-1}{k}}} & \dfrac{p_0}{p_4}>0.546\\ K_c A_5\sqrt{\dfrac{2gk}{R_g(k-1)T_4}}p_4(0.227) & \dfrac{p_0}{p_4}\le 0.546\end{cases} \quad (15)$$

The gas flow equations for other types of blowby patterns are very similar to the first pattern, and the flow direction of gas is determined by the gas pressure of the inter-ring.

There are four air chambers composed of five piston rings from top to bottom, and the gas state differential equations can be formulated,

$$\frac{dp_1}{dt}=\frac{R_gT_1}{V_1}\left(\frac{dW_i}{dt}-\frac{dW_1}{dt}\right);\ \frac{dp_2}{dt}=\frac{R_gT_2}{V_2}\left(\frac{dW_1}{dt}-\frac{dW_2}{dt}\right);$$
$$\frac{dp_3}{dt}=\frac{R_gT_3}{V_3}\left(\frac{dW_2}{dt}-\frac{dW_3}{dt}\right);\ \frac{dp_4}{dt}=\frac{R_gT_4}{V_4}\left(\frac{dW_3}{dt}-\frac{dW_4}{dt}\right) \quad (16)$$

where, K_c is the gas flow coefficient, k is the gas specific heat, R_g is the gas constant, $A_1 \sim A_5$ are the blowby area of five ring gaps respectively, and are calculated through the CAD drawings of the piston rings and the structure size of the ring gap. $V_1 \sim V_4$ are the volume of the four air chambers respectively, $W_i \sim W_4$ are the blowby among five piston ring gap respectively, $T_1 \sim T_4$ are the gas temperature of the four air chambers respectively, p_i, $p_1 \sim p_4$, p_0 are the cylinder pressure, inter-ring gas pressure and gas pressure in the crankcase respectively.

2.4. Boundary Conditions

The boundary conditions for the average Reynolds equation include inlet-outlet boundary conditions and ring gap boundary conditions. The lubricant film pressures on the inlet and outlet boundaries are assumed to be equal to the gas pressure. When the cavitation occurs, the classical Reynolds boundary condition is applied, as described in Equations (17) and (18).

$$\begin{cases}x_i=b/2,\ \bar{p}=p_1(t);\\ x_o=-b/2,\ \bar{p}=p_2(t)\\ \quad \text{in the case of sufficient lnbricant;}\\ x_o=x_c,\ \bar{p}=p_2(t),\ \partial\bar{p}/\partial x=0\\ \quad \text{in the case of cavitation.}\end{cases} \quad (17)$$

$$y=0 \text{ or } y=L,\ \bar{p}=\frac{(p_1(t)-p_2(t))}{b}x+\frac{(p_1(t)-p_2(t))}{2} \quad (18)$$

It should be noted that the gas pressures $p_1(t)$ and $p_2(t)$ at the leading and the trailing edges of piston rings change with the direction of the moving piston, and a linear variation of the gas pressure is applied from the leading edge to the trailing edge of the ring.

The three-dimensional elastohydrodynamic lubrication equation was solved by using time backward-space center difference method, and the VC++ codes were programmed successfully.

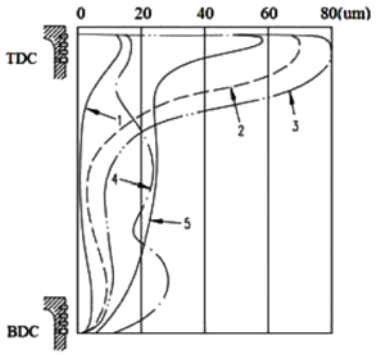

Figure 6. Wear distribution of cylinder liner.

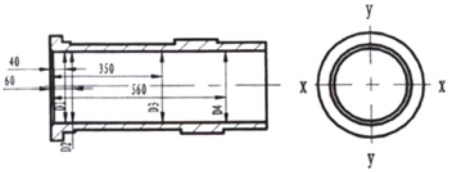

Figure 7. Wear measurement depth of cylinder liner.

3. COMPUTATIONAL MODEL OF ADHESIVE WEAR AND WEAR MEASUREMENT

There are three types of wear between piston ring and cylinder liner on diesel engines: abrasive wear, corrosion wear and adhesive wear. The wear distribution rule of the cylinder liner under different working conditions can be seen in Figure 6, curve 1 indicates the normal wear, and curve 2 denotes the abrasive wear due to lots of dust and a serious coke in the air intake, and curve 3 shows the adhesive wear, and curve 4 indicates the wear loss due to lots of metal abrasives and dust in the lubricating oil, and curve 5 means the corrosion wear due to burning high sulfur fuel when the cooling water temperature is low and frequent start under low temperature.

The adhesive wear is usually dominating in the wear of piston ring-cylinder liner. When the above EHD lubrication model was solved and the asperity contact force W_A was substituted into equation (19), as Figure 8 shows, then the wear loss of piston ring-cylinder liner were calculated respectively.

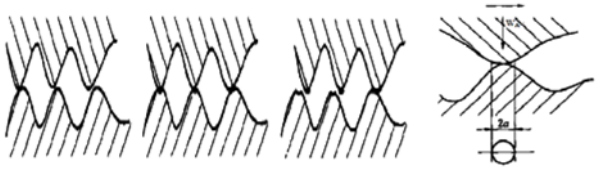

Figure 8. Adhesive wear of the piston ring-cylinder liner.

$$dV / ds = \kappa W_A / 3\sigma_s \quad (19)$$

where, dV/ds is the wear loss, and it represent with the radial wear depth of the micro unit area, σ_s is the yield limits of material, and κ is the wear constant of the lubricant. The calculated results of wear loss for the piston rings and cylinder liner will be discussed in Sections 5.1 and 5.2.

In order to verify the EHD analysis and wear calculation model, the wear measurement of cylinder liner was performed after the diesel engine worked for 400 hours. The diameter deviations of liner under different measurement depth were tested, as shown in Figure 7, and these results comparison can be seen in Section 5.3.

4. COMPUTATIONAL RESULTS OF EHD LUBRICATION AND DISCUSSION

The VC++ programs were developed according to the above EHD lubrication models, and all the related computational results were gained. Some results were changed with crank angle (φ), and the result at a crank angle of 360° (φ = 360°), namely when the piston was at the TDC, was shown in the following figures.

4.1. Inter-ring Pressure and the Blowby of Ring Gap

The corresponding gas flow differential equations and gas state differential equations were established according to the air chambers composed of piston rings and blowby patterns. The inter-ring pressure and the blowby of ring gap in a working cycle can be obtained by simultaneously solving the above first-order differential equations using Runge-Kutta method.

It can be seen from Figure 9 that the gas pressure of the inter-ring decreases from the top of the cylinder to the bottom of the cylinder liner. Figure 10 shows that the gas blowby of the first piston ring gap is larger than that of other rings. One reason is that the cylinder pressure is

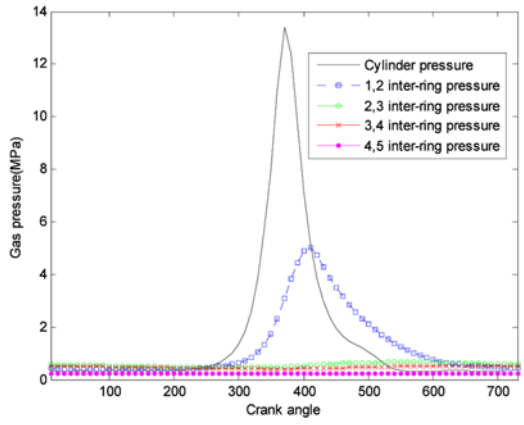

Figure 9. Cylinder pressure and calculated inter-ring pressure.

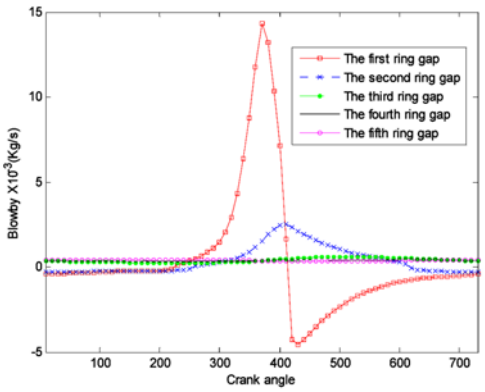

Figure 10. Blowby among ring gap.

larger than the inter-ring pressure, and the other reason is that the blowby area of the first ring is the biggest just except for the fifth piston ring.

4.2. Friction Force and Friction Heat Flux

The total friction force on the contact surface between piston ring and cylinder liner includes two parts, one is the asperity shear force, and the other is the hydrodynamic shear force. Figure 11 and Figure 12 show the distribution rules of the friction force and friction heat flux for each piston ring in a working cycle respectively. The velocity of piston and the oil film pressure have effect on the hydrodynamic shear force, the faster velocity and the higher pressure occurs, the bigger hydrodynamic shear force develops. While the asperity shear forces are generally zeroes at most of crank angles except for near the TDC and BDC, especially at the TDC when the fuels ignited. The oil film thickness has effect on the asperity shear force, the thinner oil film thickness is, and the bigger asperity shear force is.

It can be seen from Figure 11 that the hydrodynamic friction force is generally larger than the asperity friction force, and the main component of the total friction force. Both the friction heat flux and the hydrodynamic shear force are zero when the piston ring slides at the TDC and BDC, because the velocity of the piston is zero at that moment.

4.3. Oil Film Pressure

In the course of modeling, the piston ring was unfolded along the center of the ring gap, and the axial coordinate denotes the height direction of the piston ring and the zero face of axis coordinate is located in the centre face, and the circumferential coordinate denotes the circle boundary direction of piston ring or cylinder liner. The distribution of the oil film pressure on the piston rings, as shown in Figure 13, indicates that the biggest value occurs near the center of the axial direction of the ring, and the smallest value occurs at the ring gap.

In the circumferential direction, the oil film pressure was

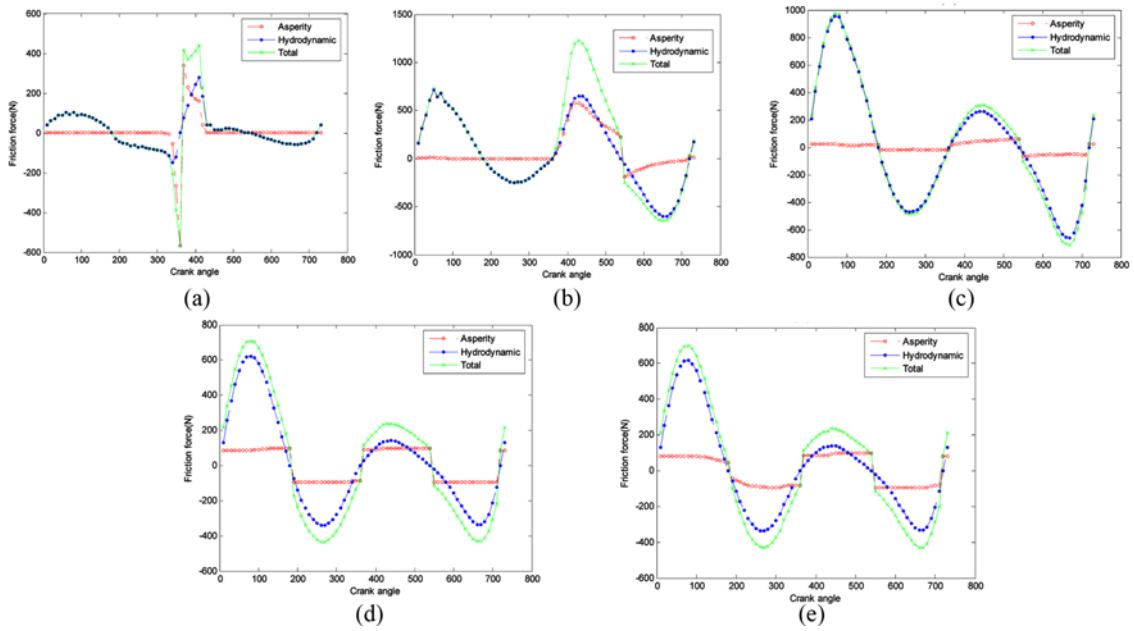

Figure 11. Friction fore of piston ring: (a) first piston ring; (b) second piston ring; (c) third piston ring; (d) fourth piston ring; (e) fifth piston ring.

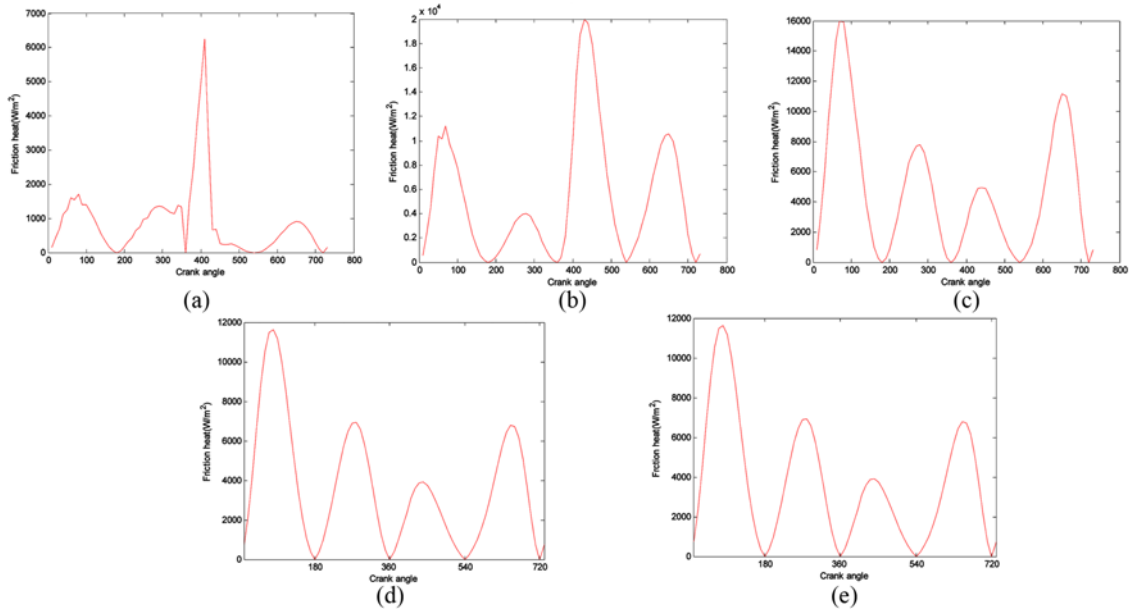

Figure 12. Friction heat flux of piston ring: (a) first piston ring; (b) second piston ring; (c) third piston ring; (d) fourth piston ring; (e) fifth piston ring.

uniform except for at the end of piston ring gap, because the interstice in this direction between cylinder liner and piston ring were equivalent. In addition, it can be found from Figure 13 that the oil film pressure in the inlet of piston ring was generally higher than that in the outlet of piston ring, because the gas pressure in the inlet was higher than that in the outlet in the axial direction of piston ring.

4.4. Minimum Oil Film Thickness

The minimum oil film thickness changed with the movement of the piston, when the velocity of the piston is fast, the minimum oil film thickness is bigger. Meanwhile, the oil film thickness is related to the gas pressure and gas temperature. Figure 14 shows the minimum oil film thickness on the piston rings.

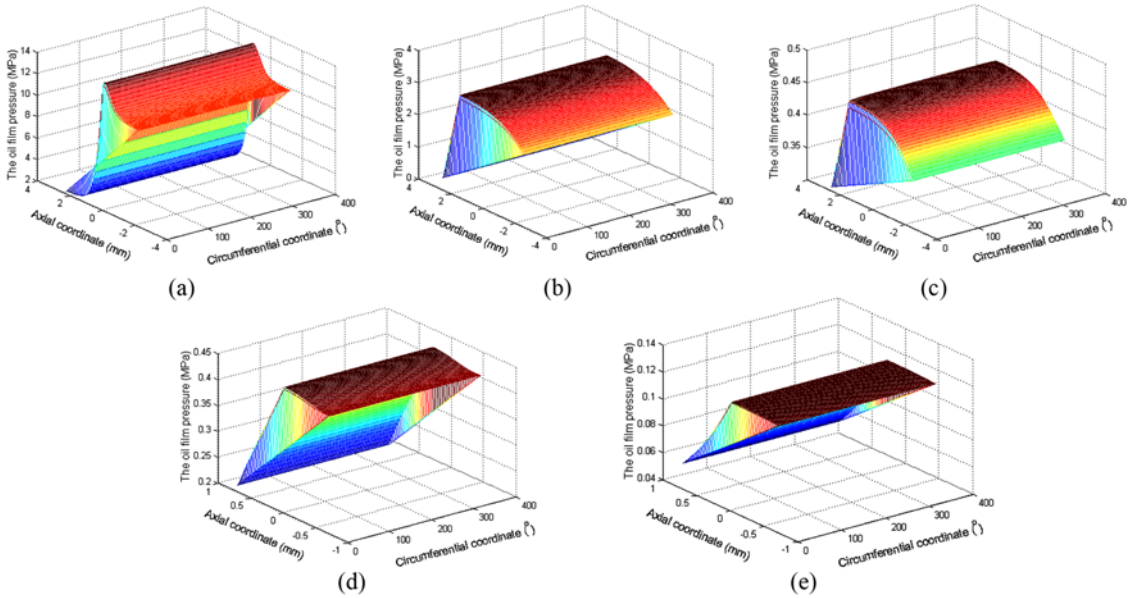

Figure 13. 3D distribution of the oil film pressure for piston ring at the TDC ($\varphi = 360^{o}$): (a) first piston ring; (b) second piston ring; (c) third piston ring; (d) fourth piston ring; (e) fifth piston ring.

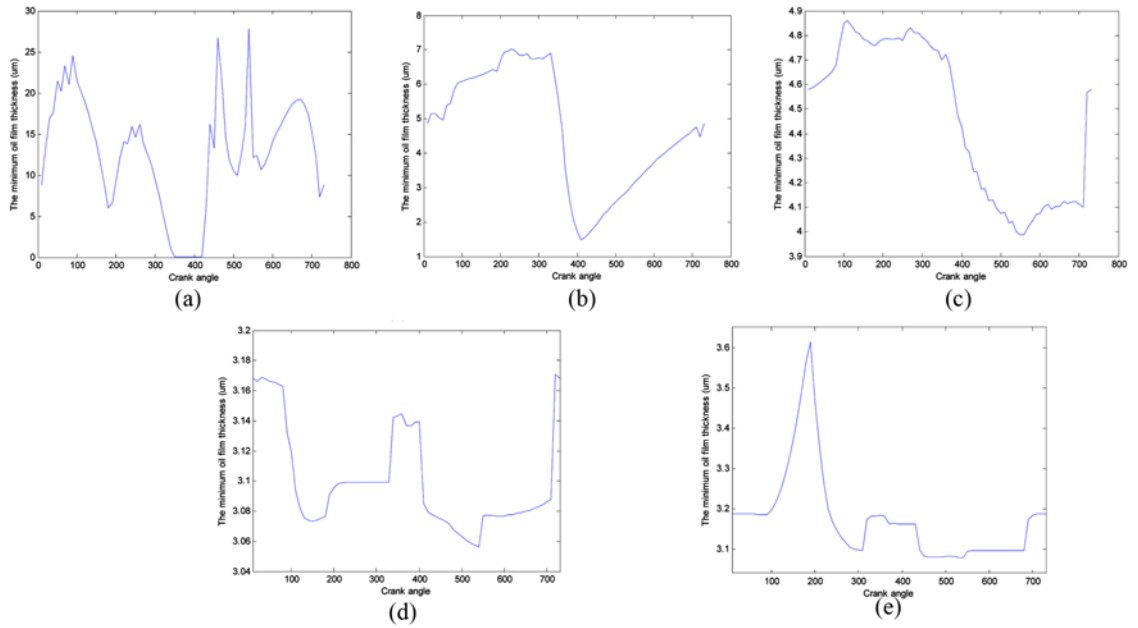

Figure 14. Minimum oil film thickness of piston ring: (a) first piston ring; (b) second piston ring; (c) third piston ring; (d) fourth piston ring; (e) fifth piston ring.

It can be noticed from Figure 14 that the minimum oil film thicknesses of the first and second piston rings occur near the TDC after the compression stroke, at a crank angle φ of about 400°. The main reason is that the velocity of piston near TDC is slower, and the gas pressure and gas temperature are higher at the same time. While the minimum oil film thicknesses of the third, the fourth and fifth piston rings occur near the BDC after power stroke, at a crank angle φ of about 540°, and the velocity of piston near TDC is also slower at this time.

4.5. Nominal Oil Film Thickness

Figure 15 shows that the nominal oil film thickness distributions of the barrel piston ring and the rectangular

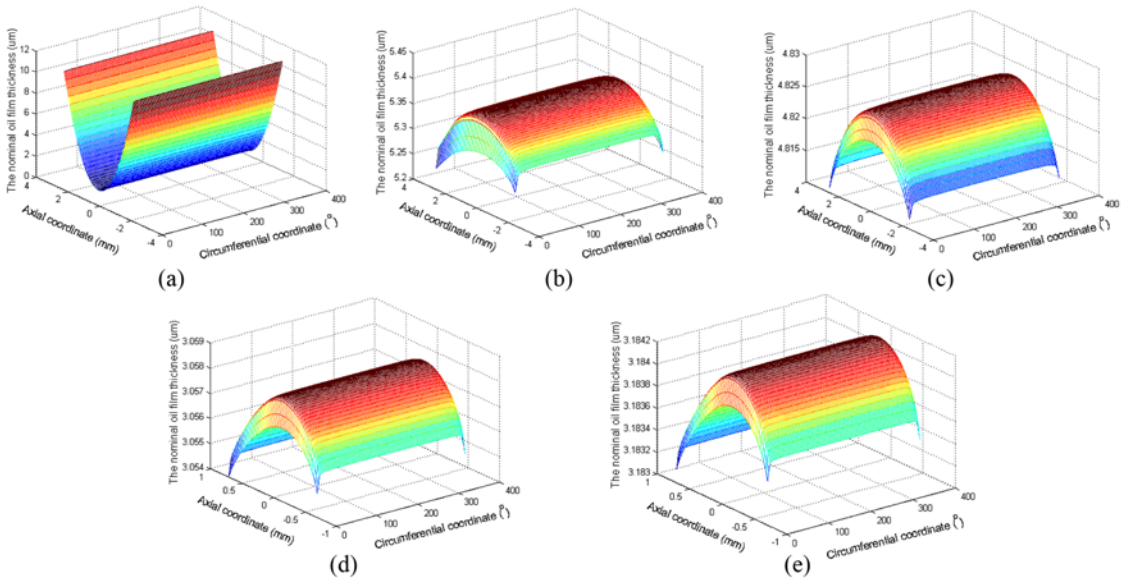

Figure 15. 3D distribution of the nominal oil film thickness for piston ring at the TDC ($\varphi = 360^{o}$): (a) first piston ring; (b) second piston ring; (c) third piston ring; (d) fourth piston ring; (e) fifth piston ring.

piston ring are very different. For the rectangular piston ring, from the second ring to the fifth ring, the distribution rule are very similar, the nominal oil film thickness at the TDC is nonuniform in the circumferential direction, and it is smaller in the ring gap than other position of piston rings, because there is a larger deformation in the gap of ring. In axial direction, the film thickness at the center of piston ring is larger than other places, but for the first piston ring, the distribution rule is opposite to them, because the first ring is a barrel ring, and there are some heights for barrel shape.

For the rectangular piston rings, the nominal oil film thickness was uniform in the circumferential direction except for at the end of piston ring gap, because the interstice in this direction between cylinder liner and piston ring were equivalent. The fluctuations of nominal oil film thickness in the circumferential direction mainly result from the elastic deformation.

4.6. The Elastic Deformation

Figure 16 shows that the distribution rules of the normal

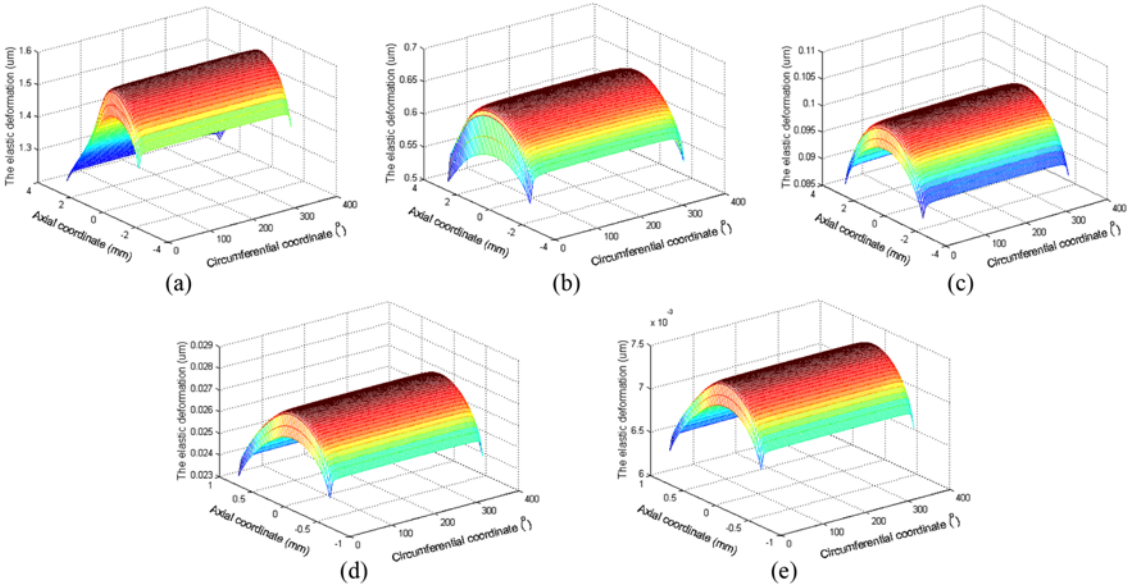

Figure 16. 3D distribution of the normal elastic deformation for piston ring at the TDC ($\varphi = 360^{o}$): (a) first piston ring; (b) second piston ring; (c) third piston ring; (d) fourth piston ring; (e) fifth piston ring.

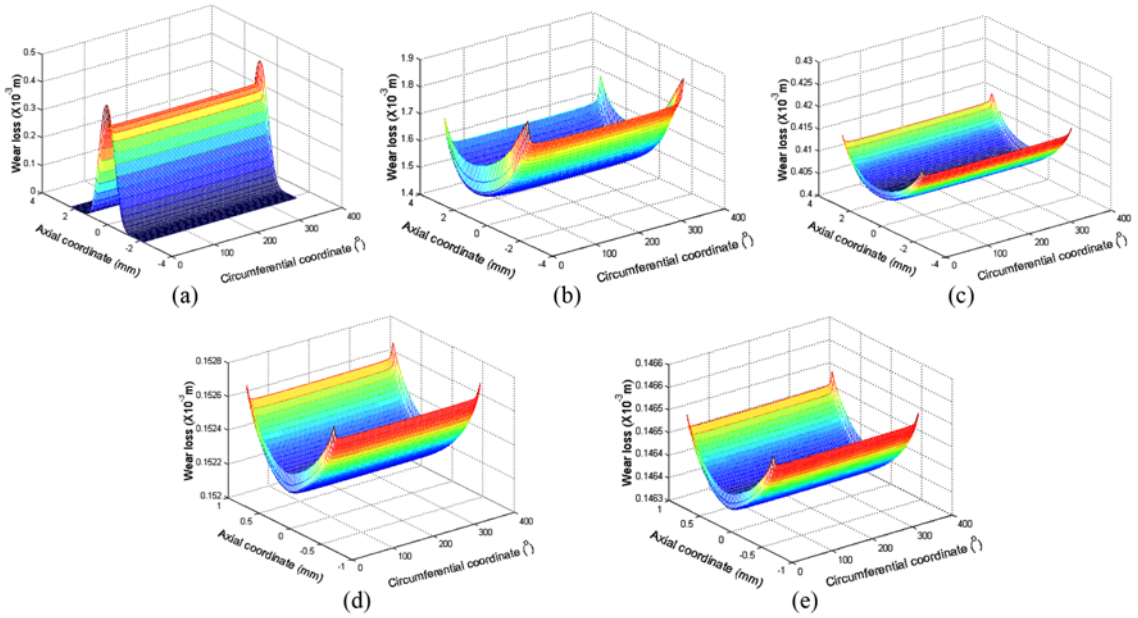

Figure 17. 3D wear loss distribution of piston ring: (a) first piston ring; (b) second piston ring; (c) third piston ring; (d) fourth piston ring; (e) fifth piston ring.

elastic deformation of piston rings are similar to the nominal oil film thickness. The elastic deformation of the piston ring is also nonuniform along the axial and circumferential directions.

The elastic deformation is decreased with the gas pressure and oil film pressure. The elastic deformation of the first piston ring is the biggest one, because the pressure near the first piston ring is higher than others. The largest deformation occurs near the center of the axial ring height, because the corresponding oil film pressure here is larger.

5. COMPUTATIONAL RESULTS OF WEAR

5.1. Wear Loss of Piston Ring

The adhesive wear loss of piston rings was calculated when the diesel engine was operated for 1000 hours under warm start condition. The five rings have different wear loss distributions, as shown in Figure 17.

Figure 17 shows that the distribution rules of the wear loss of piston rings are opposite to the nominal oil film thickness. For the rectangular piston ring (from the second ring to the fifth ring), in axial direction, the smallest wear loss occurs at the center of the piston ring; in circumferential direction, the greatest wear loss occurs at the ring gap. While for the barrel piston ring (the first ring), in axial direction, the greatest wear loss emerges at the center of piston ring; in circumferential direction, the greatest wear loss occurs at the ring gap too.

5.2. Wear Loss of Cylinder Liner

The correct EHD lubrication analysis is the precondition

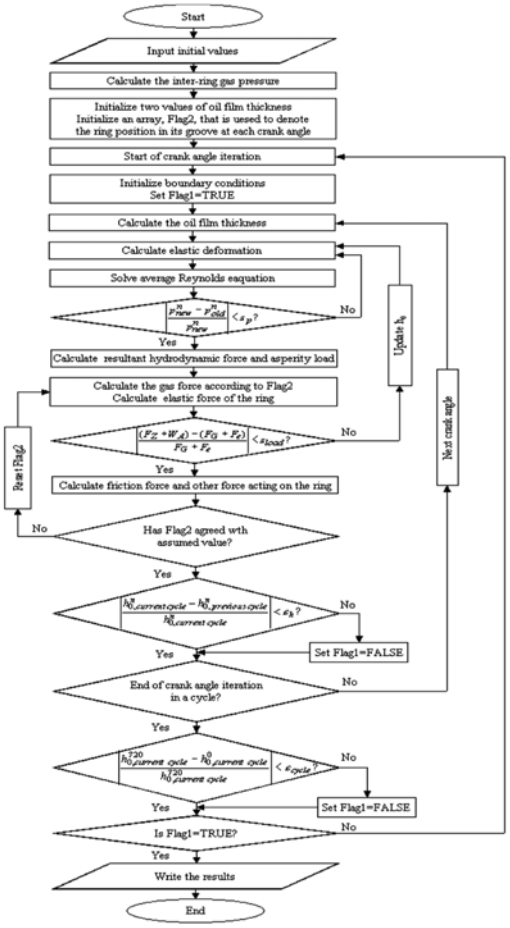

Figure 18. Procedures of the 3D EHD lubrication analysis.

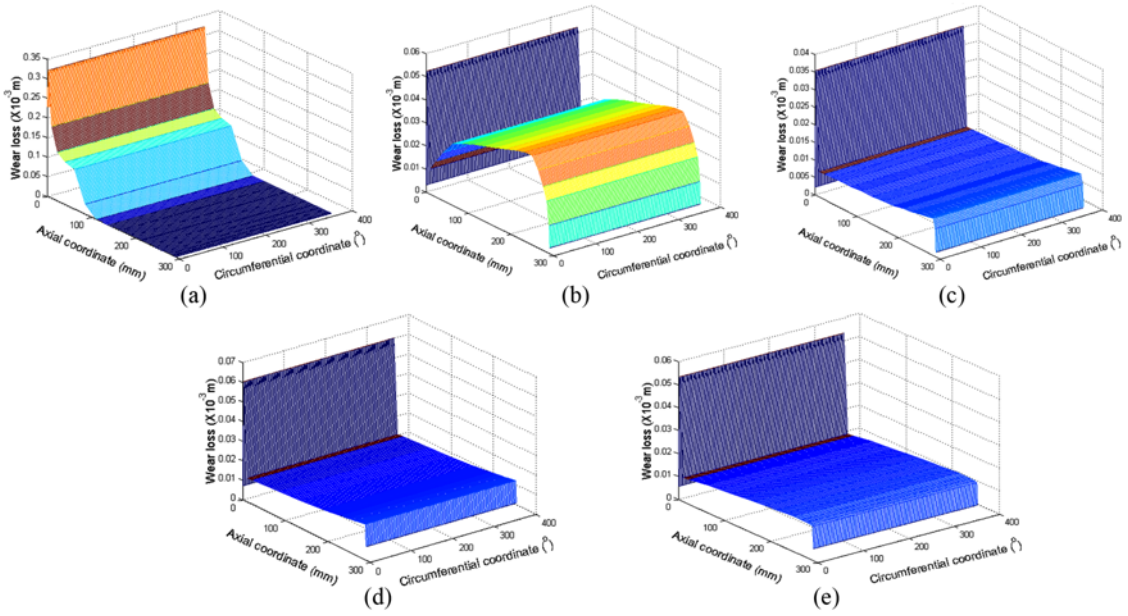

Figure 19. 3D segmental wear loss distribution of cylinder liner caused by piston rings: (a) first piston ring; (b) second piston ring; (c) third piston ring; (d) fourth piston ring; (e) fifth piston ring.

for the computation of the wear loss. The computational procedures of the present 3D EHD lubrication model were given as Figure 18, and the corresponding VC++ programs were compiled according to the above procedures. The asperity contact force W_A can be obtained through EHD lubrication analysis besides oil film pressure, friction heat, and elastic deformation. The same computation mesh was used, and then the asperity contact force W_A was substituted into equation (19) for calculating the wear loss of piston ring and cylinder liner. Finally, in order to obtain the total wear losses of the cylinder liner caused by all the five piston rings when the piston was moved from the TDC to the BDC, the segmental wear loss shown in Figure 19 should be accumulated and interpolated linearly by determining the overlap sliding regions.

Figure 19 shows the segmental wear loss of cylinder liner caused by piston rings. There is the different sliding region in the cylinder liner for every piston ring because of the spaces between piston rings, and the sliding regions were overlapped.

In order to obtain the total wear losses between the cylinder liner and the five piston rings when the piston was moved from the TDC to the BDC, the segmental wear loss shown in Figure 19 were accumulated and interpolated linearly by determining the overlap sliding regions. The results of the total wear loss of cylinder liner are shown in Figure 20. The 2D simulated result based on AVL software was used to verify the model in the present method.

Figure 19 shows that the biggest wear loss caused by each piston ring occurs near the TDC, because the higher combustion chamber gas pressure and lower sliding speed

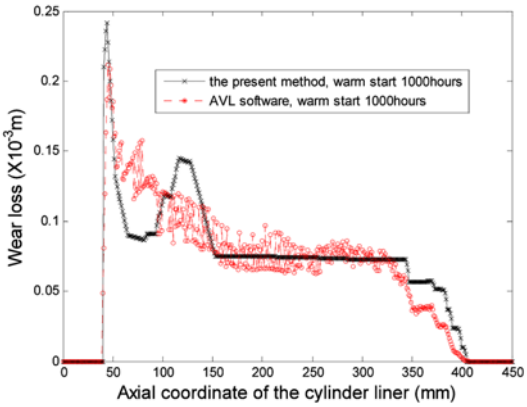

Figure 20. Total wear loss of cylinder liner using the present method and AVL software.

of the ring at that moment. The wear loss caused by the first piston ring is larger than that by other piston rings, and was dominating in the wear of the cylinder liner. Meanwhile, it can be seen from Figure 20 that the simulated pressure result agrees well with the 2D result simulated using the AVL software. It indicates that the present method is feasible.

5.3. Wear Measurement and Comparison

The wear loss of cylinder liner was calculated using the VC++ programs when the diesel engine was worked under cold start condition and warm start condition respectively. A large four-stroke, directly injected marine diesel engine was used to study the wear loss of the cylinder liner at

different startup conditions. The engine speed for measurements is 1050 r/min, the rated power is 4631 kW, detonation pressure is 13.3 MPa, and the oil used in the engine is CD40. The other characteristics of diesel engine are shown in Table 1. The calculated time for cold start condition was 150 seconds, and then the wear loss was compared with that under warm start condition. Meanwhile, the wear measurement of cylinder liner were performed several times after the diesel engine running 400 hours under warm start condition, and the corresponding calculated result was compared with the wear measurement. The wear measurements of the cylinder liner was carried out after that the diesel engine was disassembled according to Republic of China Machinery Industry Standard JB/T 9758-2004"cylinder liners, piston rings quickly wear simulation test methods".

Figure 21 shows the wear of cylinder liner under cold start condition, and the maximum wear loss of cylinder liner after the diesel engine running 150 seconds under cold start condition is about equivalent to that running 13.8 minutes under warm start condition. The wear loss under cold start condition is much larger than that under warm start condition, because the start time is very short and the continuous oil film does not form when the engine runs in this situation.

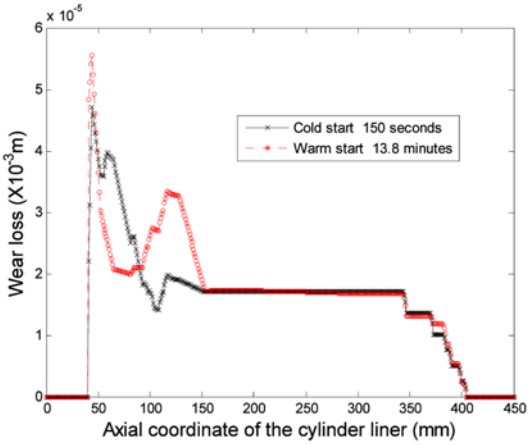

Figure 21. Comparison between warm and cold start conditions.

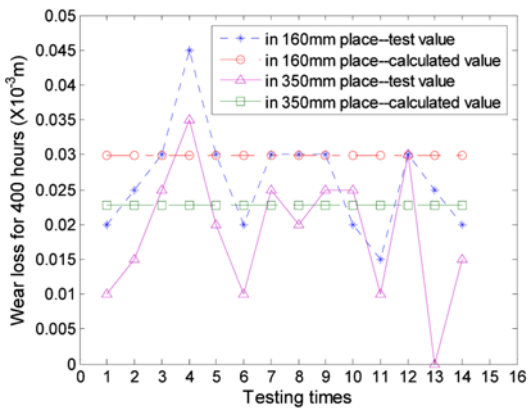

Figure 22. Comparison between simulation and test.

Table 2. Measured wear results and simulated result of cylinder liner ($\times 10^{-3}$ m).

Testing times	1	2	3	4	5
160 mm depth	0.02	0.025	0.03	0.045	0.03
350 mm depth	0.01	0.015	0.025	0.035	0.02
Testing times	6	7	8	9	10
160 mm depth	0.02	0.03	0.03	0.03	0.02
350 mm depth	0.01	0.025	0.02	0.025	0.025
Testing times	11	12	13	14	Simulated result
160 mm depth	0.015	0.03	0.025	0.02	0.030
350 mm depth	0.01	0.03	0	0.015	0.023

Figure 22 and Table 2 illustrate the comparison between the wear loss measurement of cylinder liner and simulated result. The test positions are the 160 mm depth and 350 mm depth of the cylinder liner, and every position was measured 14 times after the diesel engine running 400 hours under warm start condition. Also, it can be found here that the present simulated result matches well with the test result, especially, at 350 mm depth of the cylinder liner. Meanwhile, it is verified that the adhesive wear is usually dominating in the wear of piston ring-cylinder liner. The errors result from that the calculated value is the principal adhesive wear, while the measurements include other types of wear loss. There are some other reason for the difference between simulation results and test results. Firstly, the EHD lubrication and wear loss between the piston rings and cylinder liner are mainly considered, but the lubrication and wear between the piston skirt and cylinder liner are not considered. Secondly, the pure lubrication oil was considered during the simulation process, does not consider the effects of the liquid-solid two-phase flow caused by particulate additives, wear particles and intake dust on the lubrication friction and wear in the diesel engine. While, the test results include the total wear loss caused by all the above-mentioned factors.

6. CONCLUSION

The lubrication performance and wear loss of piston ring-cylinder liner play an important role in the reduction of the total mechanical loss in diesel engines. In the three-dimensional numerical model reported in this paper, important factors including gas blowby, oil film pressure, friction heat, and elastic deformation were considered comprehensively. The wear loss of cylinder liner under warm start condition and cold start condition was compared through simulation and experiment. By means of

the analysis and comparison, the following conclusions can be drawn.

(1) The present 3D EHD lubrication model and the VC++ programs for the lubrication and wear simulation of the piston ring-cylinder liner in the firing diesel engine are valid and feasible, as the distribution rules and trends of the amount of wear for the 3D EHD model, 2D AVL software simulation and test results are basically the same, but there are also some differences in value. The difference for the two simulation results mainly arises from the two different model simplifications. The 3D EHD model does not consider the effect of piston deflection and cylinder vibration on the lubrication friction and wear since the complex tribological systems, but in the commercial software AVL, these factors are taken into consideration in the 2D model.

(2) The lubrication and wear calculation of the diesel engine with five piston rings is more complicated than that of a gasoline engine due to the complex blowby patterns and inter-ring pressure. The gas blowby, the friction heat and the elastic deformation have a great effect on the lubrication results, and these factors must be considered together.

(3) It has been found that the 3D distribution of the oil film pressure, the nominal oil film thickness, the normal elastic deformation and wear loss were not uniform in the circumferential direction. The distribution patterns of the normal elastic deformation are similar to that of the nominal oil film thickness. However the distribution patterns of the wear loss of the piston rings are opposite to that of the nominal oil film thickness.

(4) The hydrodynamic friction force is larger than the asperity friction force on the lubrication interface, and it is the main component of the total friction force. The distribution pattern of the barrel piston ring is very different from that of the rectangular piston ring. The top first barrel piston ring plays a dominant role in the wear loss of the cylinder liner, and the maximum wear loss of cylinder liner occurs near the vicinity of TDC.

(5) Since the starting time was very short and the condition in which continuous oil film was not reached yet in this modeling, the wear of cylinder liner under cold start condition is much larger than that under warm start condition. For this example, the maximum wear loss of cylinder liner after the diesel engine running 150 seconds under cold start condition was about equivalent to that running 13.8 minutes under warm start condition.

The calculation results will be provided for engineers to improve the reliability and service life of the diesel engine, and enhance the design of the piston ring and cylinder liner. The future study is to develop the real-time measurement system of the oil film thickness and friction force, and consider the antifriction and antiwear effect of nanometer additive in lubricant for engine.

ACKNOWLEDGEMENT–The Project were supported by State Key Laboratory of Engines, Tianjin University (K2012-08) and the Scientific Research Foundation for the Returned Overseas Chinese Scholars, State Education Ministry, [2011]1139. The financial support to the authors is gratefully acknowledged.

REFERENCES

Charles, P., Elfassi, M. and Lubrecht, A. A. (2010). Double-Newtonian rheology in a model piston-ring cylinder-wall contact. *Tribology Int.* **43**, **10**, 1902–1907.

Cho, S. W., Choi, S. M. and Bae, C. S. (2000). Frictional modes of barrel shaped piston rings under flooded lubrication. *Tribology Int.* **33**, **8**, 545–551.

Choi, J., Kim, S. S., Rhim, S. S. and Choi, J. H. (2012). Numerical modeling of journal bearing considering both elastohydrodynamic lubrication and multi-flexible-body dynamics. *Int. J. Automotive Technology* **13**, **2**, 255–261.

Chong, W. W. F., Teodorescu, M. and Vaughan, N. D. (2011). Cavitation induced starvation for piston-ring/liner tribological conjunction. *Tribology Int.* **44**, **4**, 483–497.

Dhara, A., Agarwal, A. K. and Saxena, V. (2009). Measurement of dynamic lubricating oil film thickness between piston ring and liner in a motored engine. *Sensors and Actuators A: Physical* **149**, **1**, 7–15.

Jiang, Y. K., Liu, Z. E., Reitz, R. D., Dong, Z. L. and Ye, X. M. (2007). Improvement of transient heat transfer models for the coupled 3-D moving piston assembly-liner system. *Proc. ASME Int. Mechanical Engineering Cong. and Exposition* 2007, Seattle, United States, 547–554.

Johansson, S., Nilsson, P. H., Ohlsson, R. and Rosén, B. G. (2011). Experimental friction evaluation of cylinder liner/piston ring contact. *Wear* **271**, **3–4**, 625–633.

Kapsiz, M., Durat, M. and Ficici, F. (2011). Friction and wear studies between cylinder liner and piston ring pair using Taguchi design method. *Advances in Engineering Software* **42**, **8**, 595–603.

Liu, K., Xie, Y. B. and Gui, C. L. (1998). Two-dimensional lubrication study of the piston ring pack. *Proc. Institution of Mechanical Engineers, Part J: J. Engineering Tribology* **212**, **3**, 215–220.

Livanos, G. A. and Kyrtatos, N. P. (2007). Friction model of a marine diesel engine piston assembly. *Tribology Int.* **40**, **10–12**, 1441–1453.

Ma, M. T., Sherrington, I., Smith, E. H. and Grice, N. (1997). Development of a detailed model for piston-ring lubrication in IC engines with circular and non-circular cylinder bores. *Tribology Int.* **30**, **11**, 779–788.

Michalski, J. and Wos, P. (2011). The effect of cylinder liner surface topography on abrasive wear of piston-cylinder assembly in combustion engine. *Wear* **271**, **3–4**, 582–589.

Qasim, S. A., Afzaal, M. M., Alikhan, M. and Mufti, R. A.

(2011). Low viscosity shear heating in piston skirts EHL in the low initial engine start up speeds. *Tribology Int.* **44**, **10**, 1134–1143.

Stark, M. S., Gamble, R. J., Hammond, C. J., Gillespie, H. M., Lindsay Smith, J. R., Nagatomi, E., Priest, M., Taylor, C. M., Taylor, R. I. and Waddington, D. J. (2005). Measurement of lubricant flow in a gasoline engine. *Tribology Letters* **19**, **3**, 163–168.

Tamminen, J., Sandstrom, C. E. and Andersson, P. (2006). Influence of load on the tribological conditions in piston ring and cylinder liner contacts in a medium-speed diesel engine. *Tribology Int.* **39**, **12**, 1643–1652.

Truhan, J. J., Qu, J. and Blau, P. J. (2005). A rig test to measure friction and wear of heavy duty diesel engine piston rings and cylinder liners using realistic lubricants. *Tribology Int.* **38**, **3**, 211–218.

Yang, Q. M. and Keith, T. G. Jr. (1996a). Two-dimensional piston ring lubrication-part I: rigid ring and liner solution. *Tribology Transaction* **39**, **4**, 757–768.

Yang, Q. M. and Keith, T. G. Jr. (1996b). Two-dimensional piston ring lubrication-Part II: elastic ring consideration. *Tribology Trans.* **39**, **4**, 870–880.

Ye, X. M., Chen, G. H., Jiang, Y. K. and Zou, Y. C. (2004). Numerical investigation of the EHL performance and friction heat transfer in piston and cylinder liner system. *SAE Paper No.* 2004-01-0778.

Ye, X. M., Chen, G. H., Luo, M. J. and Jiang, Y. K. (2003). Three-dimensional analysis of tribological performance and heat transfer in piston and cylinder liner system. *ASME Int. Combus. Engine Div. Publ ICE*, **40**, 351–361.

Zhang, J. P., Jiang, Y. K., Liu, X. and Dong, Z. L. (2010). 3-D numerical simulation and experimental study on the wear of piston ring-cylinder liner. *Advanced Material Research*, **139**–**141**, 1036–1039.